



Single-pulse interference caused by temporal reflection at moving refractive-index boundaries

BRENT W. PLANSINIS,^{1,2,*} WILLIAM R. DONALDSON,² AND GOVIND P. AGRAWAL^{1,2}

¹The Institute of Optics, University of Rochester, Rochester, New York 14627, USA

²Laboratory for Laser Energetics, University of Rochester, 250 E. River Road, Rochester, New York 14623, USA

*Corresponding author: bplansin@ur.rochester.edu

Received 8 June 2017; revised 16 August 2017; accepted 1 September 2017; posted 7 September 2017 (Doc. ID 296906); published 29 September 2017

We show numerically and analytically that temporal reflections from a moving refractive-index boundary act as an analog of Lloyd's mirror, allowing a single pulse to produce interference fringes in time as it propagates inside a dispersive medium. This interference can be viewed as the pulse interfering with a virtual pulse that is identical to the first, except for a π -phase shift. Furthermore, if a second moving refractive-index boundary is added to create the analog of an optical waveguide, a single pulse can be self-imaged or made to produce two or more pulses by adjusting the propagation length in a process similar to the Talbot effect. © 2017 Optical Society of America

OCIS codes: (320.5550) Pulses; (060.5530) Pulse propagation and temporal solitons; (320.0320) Ultrafast optics.

<https://doi.org/10.1364/JOSAB.34.002274>

1. INTRODUCTION

Double-slit interference, which occurs when light exiting from two closely spaced, narrow slits forms intensity fringes in a plane transverse to the direction of light propagation, has been a cornerstone of the wave nature of light for centuries [1]. Its temporal analog, where two short pulses propagate through a dispersive medium and form interference fringes in time, has also been explored through the well-known space–time analogy [2–4].

Recently, there has been a growing interest in temporal reflection and refraction from a moving refractive-index boundary [5–8], particularly with regards to photon acceleration [9,10], analog gravity [11–17], and interaction of solitons with dispersive waves [18–25]. In this process, a single optical pulse splits into a reflected pulse and a refracted pulse, each propagating at a different speed, after it arrives at the refractive-index boundary. The change in group velocity is caused by a splitting of the pulse spectrum [8,22,26,27].

One useful tool that combines the double-slit interference with reflection is the Lloyd's mirror configuration. In this case, diffracted light from a single slit is reflected from a mirror, creating an interference pattern that appears as if the initial slit was interfering with a virtual second slit that has a π -phase shift [28]. This configuration has seen use in photolithography [29], test-pattern generation [30], and radio astronomy [31]. However, a temporal analog of this arrangement has not yet been explored. In this paper, we show how temporal reflection from a moving refractive-index boundary leads to an analog of Lloyd's mirror for optical pulses propagating inside a dispersive

medium. We also discuss how this configuration relates to two-pulse interference in time.

The paper is organized as follows. In Section 2, we review two-pulse interference and its relation to the spatial counterpart making use of two slits. In Section 3, we discuss how a temporal analog of Lloyd's mirror is formed when an optical pulse reflects from a moving refractive-index boundary. In Section 4, we consider the temporal waveguide configuration [32] and discuss how it can be employed for either self-imaging or generation of a burst of pulses from a single pulse. The main results are summarized in Section 5.

2. TWO-PULSE INTERFERENCE

We first discuss how two large-bandwidth, temporally separated pulses propagating inside a dispersive medium can overlap in time as they broaden due to group-velocity dispersion (GVD) and form interference fringes that mimic a double-slit diffraction pattern. We consider optical pulses in the form of plane waves in the transverse spatial direction. Each frequency component of the pulses travels with a propagation constant, $\beta(\omega) = n(\omega)\omega/c$, where $n(\omega)$ is the refractive index at frequency ω . For pulses containing multiple optical cycles, $\beta(\omega)$ can be approximated by a Taylor expansion around the central frequency of the pulse such that

$$\beta(\omega) = \beta_0 + \beta_1(\omega - \omega_0) + \frac{\beta_2}{2}(\omega - \omega_0)^2, \quad (1)$$

where $\beta_m = (d^m\beta/d\omega^m)_{\omega=\omega_0}$. The parameter β_1 is the inverse of the pulses' group velocity. We simplify the following analysis

by using the retarded time, $t = T - z\beta_1$, giving us a moving-frame dispersion relation in the form

$$\beta'(\omega) = \beta_0 + \frac{\beta_2}{2}(\omega - \omega_0)^2. \quad (2)$$

Using the dispersion relation in Eq. (2), together with Maxwell's equations and the slowly varying envelope approximation, we obtain the time-domain equation

$$\frac{\partial A}{\partial z} + \frac{i\beta_2}{2} \frac{\partial^2 A}{\partial t^2} = 0, \quad (3)$$

where $A(z, t)$ is the temporal envelope of the electric field at distance z . This equation is easily solved in the frequency domain using the Fourier transform method, and the solution is given by [33]

$$A(z, t) = \int_{-\infty}^{\infty} \tilde{A}(0, \omega) \exp \left[i \frac{\beta_2 z}{2} (\omega - \omega_0)^2 - i\omega t \right] d\omega, \quad (4)$$

where $\tilde{A}(0, \omega)$ is the Fourier transform of $A(0, t)$.

The integral in Eq. (4) can be performed in a closed form in only a few special cases. However, similar to the case of far-field diffraction of optical beams, we can solve this equation analytically for large propagation distances, $z \gg 0$, or in other words, when we satisfy the far-field condition $(|\beta_2|z)^{-1} \ll \Omega_w^2$, where Ω_w is a measure of the width of the input-pulse spectrum. As is well known, the output envelope in this limit mimics the shape of the input spectrum and has the form [4,34]

$$A(z, t) = \tilde{A} \left(0, \Omega = \frac{t}{\beta_2 z} \right) \exp \left(-i \frac{t^2}{2\beta_2 z} \right). \quad (5)$$

Note that the scaling factor between the frequency and time scales is simply the group delay dispersion, $\beta_2 z$.

We now assume that the temporal waveform at $z = 0$ consists of two identical pulses separated in time by T_s :

$$A(0, t) = A_0(t - T_s/2) + A_0(t + T_s/2), \quad (6)$$

where $A_0(t)$ governs the shape of each optical pulse. By performing the Fourier transform, it is easy to show that the input spectrum is given by

$$\tilde{A}(0, \omega) = 2\tilde{A}_0(\omega) \cos(\omega T_s/2), \quad (7)$$

where \tilde{A}_0 is the Fourier transform of $A_0(t)$. It follows from the solution in Eq. (6) that when the two pulses are propagated through a long-enough dispersive medium to satisfy the far-field limit, the output intensity, $|A(z, t)|^2$, will have the form

$$|A(z, t)|^2 = 4|\tilde{A}_0|^2 \cos^2 \left(\frac{T_s t}{2\beta_2 z} \right). \quad (8)$$

The cosine term in Eq. (8) leads to the formation of interference fringes in time, with a fringe separation of $T_f = 2\pi\beta_2 z/T_s$. As the initial pulses (slits) are separated more in time, the fringes get closer together. Also, as the propagation distance, z , is increased, the fringe separation increases. This behavior is exactly analogous to the fringe separation seen in a double-slit diffraction pattern.

Figure 1 shows three simulations depicting the propagation of two hyperbolic-secant-shaped pulses propagating inside a dispersive medium with $\beta_2 = 0.05$ ps²/m. Specifically, we solved Eq. (3) with the input field of the form

$$A(0, t) = \text{sech} \left(\frac{t - T_s/2}{T_0} \right) + \text{sech} \left(\frac{t + T_s/2}{T_0} \right) \exp(i\phi), \quad (9)$$

where T_0 is related to the pulse width, and ϕ is the phase offset between the two pulses. We choose $T_0 = 0.3$ ps, giving a dispersion length ($L_D = T_0^2/|\beta_2|$) of 1.8 m and satisfying the far-field condition above. We varied T_s and ϕ such that $T_s = 2.5$ ps, $\phi = 0$ for the first column; $T_s = 5$ ps, $\phi = 0$ for the second column; and $T_s = 5$ ps, $\phi = \pi$ for the third column. The bottom row shows the evolution of the pulse shape over 100 m on a decibel scale, and the top row shows the output pulse shape on a linear scale to more clearly mark the peak position. In all cases, the two pulses broaden quickly due to group-velocity dispersion. As the dispersed pulses begin to overlap in time, they form interference fringes in a fan-like shape, appearing to form multiple pulses. As predicted by Eq. (8), a wider separation of input pulses in Fig. 1(b) leads to a smaller fringe spacing at the output, compared to Fig. 1(a).

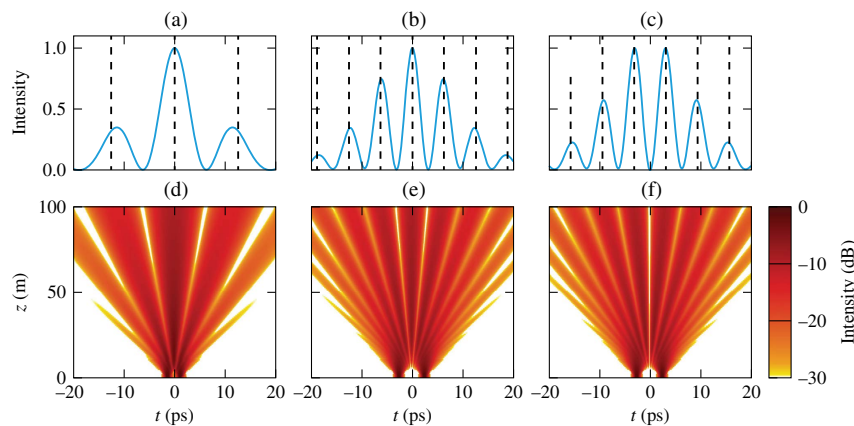


Fig. 1. (a)–(c) Output pulse shapes for two hyperbolic-secant pulses propagating in a dispersive medium with initial pulse separations of (a) $T_s = 2.5$ ps, (b) $T_s = 5$ ps, and (c) $T_s = 5$ ps. The initial pulses in (c) have a π -phase offset. The predicted fringe locations are marked with dashed black lines. (d)–(f) Evolution of pulse shape for the same pulses demonstrating the fan-like interference fringes similar to those from a double slit.

The locations of fringe peaks in both Figs. 1(a) and 1(b) do not perfectly match the values predicted by Eq. (8) (dashed black lines), because the sinusoidal modulation is contained within the envelope of the initial pulse spectrum, resulting in a slight shift of the peaks of the interference fringes from the predicted times.

We next consider the case shown in the last column of Fig. 1, where the second pulse is identical to the first but has a phase offset of $\phi = \pi$. In this case, it is easily shown that the cosine term in Eq. (7) becomes a sine term, and the output has the form

$$|A(z, t)|^2 = 4|\tilde{A}_0|^2 \sin^2\left(\frac{T_s t}{2\beta_2 z}\right). \quad (10)$$

As seen in Fig. 1(c), although the fringe spacing is the same as in Fig. 1(b), the locations of the “bright” and “dark” fringes have been reversed. This makes sense because bright and dark fringes differ by a phase shift of π . Figure 1(f) shows the propagation of the same two pulses as in Fig. 1(e), except for a relative phase shift of $\phi = \pi$. Again, we see the pulses quickly broaden due to the GVD of the dispersive medium and form interference fringes. But, as predicted, the bright and dark fringes have swapped locations, compared to the $\phi = 0$ case.

3. SELF-INTERFERENCE CAUSED BY TIME REFLECTION

In this section, we consider the temporal reflection of an optical pulse inside a dispersive medium from a single moving refractive-index boundary. For simplicity, we use a reference frame that is moving with the boundary such that $t = T - z/v_B$, where v_B is the speed of the boundary. We also Taylor-expand the dispersion relation around a frequency whose group velocity matches the speed of the temporal boundary. Similar to the derivation of the nonlinear Schrödinger equation inside a dispersive nonlinear medium, we introduce two time scales, a fast one at which the electric field oscillates and a slower one at which the amplitude envelope varies [33,35]. Assuming that the temporal transition region occurs on the slow time scale (>10 optical cycles), the evolution of the pulse envelope is governed by

$$\frac{\partial A}{\partial z} + \frac{i\beta_2}{2} \frac{\partial^2 A}{\partial t^2} = i\beta_B(t)A, \quad (11)$$

where $\beta_B(t) = k_0 \Delta n(t)$ is the shift in the dispersion curve caused by a time-dependent refractive-index change of $\Delta n(t)$. Physically speaking, the dispersion relation of the medium before the temporal boundary is the same as in Eq. (2), and, after the temporal boundary, takes the form [8,32]

$$\beta'(\omega) = \beta_0 + \frac{\beta_2}{2}(\omega - \omega_0)^2 + \beta_{B0}, \quad (12)$$

where β_{B0} is a constant shift of the dispersion curve caused by the active process used to create the refractive-index shift. Note that the dispersion relation before and after the boundary corresponds to propagation in two homogeneous media, with a transition between the two located at T_B .

We stress that the moving refractive-index boundary is actually a temporal transition region, where the refractive index changes over a few optical cycles. An actual step-like boundary

would cause a nonadiabatic transition, which would scatter between bands of the medium [36]. However, as long as the rise time of this transition region is much shorter than the duration of the optical pulse, while still being longer than a few optical cycles, we can safely approximate the transition region as a step-like boundary. This approximation requires that the change of the dispersion parameters across the transition region be small relative to their values [37], a condition that must also be satisfied in deriving Eq. (11).

In the retarded time frame, the moving refractive-index boundary becomes a stationary temporal boundary, which appears to change the refractive index for all of space and breaks translational symmetry in time [5]. Therefore, any light that crosses the boundary must satisfy conservation of momentum in the moving frame, while the frequency is free to change [5,8]. Equivalently, the moving-frame dispersion relation must be continuous across the boundary such that $\beta'(t = T_B^-) = \beta'(t = T_B^+)$. Imposing this condition, we can solve for the reflected and transmitted pulse frequencies as

$$\Delta\omega_r = -\Delta\omega_i, \quad \Delta\omega_t = \Delta\omega_i \sqrt{1 - \frac{2\beta_B}{\beta_2(\Delta\omega_i)^2}}, \quad (13)$$

where $\Delta\omega_j = \omega_j - \omega_0$. When $2\beta_B > \beta_2 \Delta\omega_i^2$, the transmitted frequency becomes imaginary, which does not correspond to a traveling solution. Therefore, all of the pulse energy must be reflected, creating a temporal analog of total internal reflection (TIR). In other words, the temporal boundary acts like a perfect mirror [8]. Note that the imaginary transmitted frequency produces a decaying exponential tail, which is analogous to the evanescent wave [8].

We solved Eq. (11) numerically using the standard split-step Fourier method. Figure 2 shows the evolution of the shape [Fig. 2(b)] and spectrum [Fig. 2(c)] over 100 m of a single sech-shaped pulse launched with $T_0 = 0.3$ ps and $\Delta\omega_i = 0$, with a temporal boundary located at $T_B = 0$. The pulse is offset from the boundary by $T_s/2 = 2.5$ ps. The parameter $\beta_B = 2.5 \text{ m}^{-1}$ was chosen to ensure TIR at the boundary over the pulse bandwidth.

We can visually see that the TIR condition is satisfied by examining Fig. 2(d), which shows the initial dispersion curve for $t < 0$ in solid blue and the shifted dispersion curve for $t > 0$ in dashed red. Because momentum must be conserved at the boundary, frequencies must maintain the same value of β' when interacting with the boundary. Because the pulse starts in the $t < 0$ region, all frequencies must begin with a value of β' on the blue curve. To be transmitted across the boundary, a given frequency must have a β' that is greater than the minimum of the red curve (shown with a dotted black line). We can easily see that there are no frequencies on the blue curve for which β' exceeds this value for the entire pulse spectrum shown in Fig. 2(c). Therefore, no frequencies can be transmitted across the boundary, and TIR must occur. Note, however, that only frequencies $(\nu - \nu_0) > 0$ will actually interact with the boundary and undergo TIR, while frequencies $(\nu - \nu_0) < 0$ have group velocities that take them away from the boundary.

Comparing Fig. 2 to Fig. 1, the fringe pattern we obtained in Fig. 2(b) appears to most closely match the case shown in Fig. 1(f), where the second pulse has a π -phase shift from the

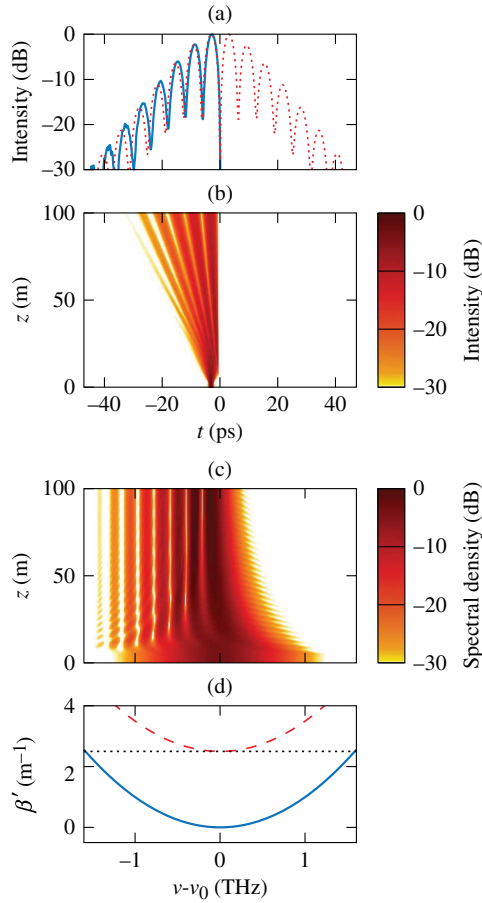


Fig. 2. (a) Fringe pattern after propagating 100 m for a single sech-shaped pulse with $T_0 = 0.3$ ps (solid blue curve). The pulse is offset initially by 2.5 ps from a co-propagating refractive-index boundary. The two-pulse fringe pattern seen in Fig. 1(c) is represented by the dotted red curve. Evolution of the (b) shape and (c) spectrum of the single sech-shaped pulse propagating with the moving refractive-index boundary. (d) Dispersion curves for $t < 0$ (solid blue curve) and $t > 0$ (dashed red curve). The dashed black curve shows the minimum initial momentum needed to cross the boundary.

first pulse. This is analogous to the Lloyd's mirror configuration, which produces interference fringes using a single slit and a mirror [28]. Because we employed a temporal analog of reflection [2,8], it is not surprising that TIR from a temporal boundary produces a π -phase shift. Indeed, a π -phase shift also occurs during traditional TIR when the angle between the surface plane and the wave vector is small. As this angle becomes larger, however, the phase shift begins to drop from π to zero. Therefore, we should expect to see a frequency-dependent phase shift across the temporal fringes. We can infer this effect by more closely examining the fringes in Fig. 2. Figure 2(a) compares the temporal fringe pattern obtained through TIR (solid blue curve) with the one in Fig. 1(c) (dotted red curve) obtained through two-pulse interference [on a decibel (dB) scale]. For times close to $t = 0$, the fringe spacing agrees extremely well in the two cases, indicating that a π -phase shift occurs during the TIR. As we get farther from $t = 0$, the bright fringes for the reflected pulse (solid blue curve) begin to shift

inward toward the dark fringes of the dotted red curve because of a reduced phase shift.

To quantify the preceding numerical behavior analytically, we need to find the phase shift, ϕ_r , added to the pulse when it reflects off of the temporal boundary. To find this phase, we must first derive the temporal analogs of the Fresnel equations. To that end, we write the total electric field of a specific frequency component before and after the boundary as (assuming linear polarization)

$$E(t) = \begin{cases} A_i e^{i(\beta' z - \Delta\omega_i t)} + A_r e^{i(\beta' z - \Delta\omega_r t)} & t < 0, \\ A_t e^{i(\beta' z - \Delta\omega_t t)} & t > 0, \end{cases} \quad (14)$$

where A_i , A_r , and A_t are the incident, reflected, and transmitted amplitudes, respectively. We now apply the boundary conditions that the electric field, $E(t)$, and its derivative, $\partial E/\partial t$, be continuous across the temporal boundary [32]. Recalling that β' is conserved in the moving frame across a temporal boundary, the boundary conditions are satisfied when

$$A_i + A_r = A_t, \quad \Delta\omega_i A_i + \Delta\omega_r A_r = \Delta\omega_t A_t. \quad (15)$$

Solving these equations, the reflection coefficient, $r = A_r/A_i$, is found to be

$$r = \frac{\Delta\omega_r - \Delta\omega_i}{\Delta\omega_r - \Delta\omega_t}. \quad (16)$$

Substituting the reflected and transmitted frequencies from Eq. (13) into Eq. (16), we find the temporal analog for the Fresnel reflection coefficient in a dispersive medium given by

$$r = \frac{1 - i\sqrt{Q-1}}{1 + i\sqrt{Q-1}}, \quad Q = \frac{2\beta_B}{\beta_2(\Delta\omega_i)^2}, \quad (17)$$

where we have assumed that the TIR condition is satisfied. In the following discussion, we focus only on the phase of the reflection coefficient since that is what determines the timing of the interference fringes. Note that when the TIR condition is satisfied, the magnitude of the reflection coefficient is unity ($|r|^2 = 1$), as expected.

From Eq. (17) we obtain the following analytic expression for the phase ϕ_r imparted to the reflected pulse during TIR:

$$\phi_r = -2 \tan^{-1}(\sqrt{Q-1}). \quad (18)$$

Figure 3(a) shows a plot of ϕ_r versus $\nu = \omega/2\pi$ for the same parameters used in Fig. 2. We see that the phase varies over the pulse spectrum as expected, starting at $\phi_r = -\pi$ near $\nu = \nu_0$ and going to zero when $|\nu - \nu_0| = 1.42$ THz. This is analogous to the phase behavior for traditional TIR. We can verify that the analytical prediction agrees with our numerical simulations using the double-slit analogy with a virtual reflected pulse. Figure 3(b) shows the output pulse shape for the reflected pulse (solid blue curve), and the dotted red curve shows the output for two interfering pulses when the reflection phase from Eq. (18) is applied to the second pulse. As the figure shows, the two sets of fringes overlap perfectly for $t < 0$, indicating that the phase shift predicted by Eq. (18) is correct. The fringes for $t > 0$ do not exist in the TIR case because both the reflected and initial pulses are trapped in the $t < 0$ region.

Interference of a reflected pulse with the unreflected parts of the initial pulse has been previously seen in a numerical study

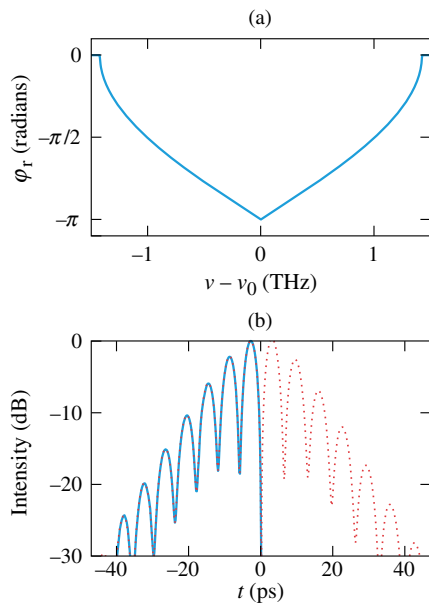


Fig. 3. (a) Total internal reflection (TIR) phase shift plotted as a function of frequency. (b) Output pulse shapes in the cases of a single pulse (solid blue curve) and two pulses (dotted red curve). The two fringe patterns match when the frequency-dependent phase shift, ϕ_r , is applied to the second pulse.

devoted to propagation of solitons inside a dispersive nonlinear medium [38]. In this study, a dispersive wave reflected off of a temporal soliton. The effect was incorrectly attributed to scattering of the dispersive wave from the soliton, rather than an interference pattern formed by the initial pulse and the temporally reflected pulse.

4. SELF-IMAGING IN A TEMPORAL WAVEGUIDE

In this section, we add a second temporal boundary such that the input pulse is located between the two boundaries, forming a temporal waveguide [15,26,32]. In this configuration, multiple reflections occur through successive TIR at the two boundaries, and we expect that infinitely many virtual pulses will interfere with the original pulse, rather than just one. This situation is analogous to the Talbot effect, and we should expect that the temporal Talbot effect will lead to self-imaging of the original pulse at certain distances [39]. Some changes are also expected, since, unlike the traditional Talbot effect where all fields are in-phase, the waveguide produces a phase shift of approximately π between adjacent pulses.

As an example, Fig. 4 shows the evolution of a pulse train when adjacent pulses differ in phase by π . As the pulses overlap in time, they quickly interfere and briefly form fringes that eventually form distinct pulses at a higher repetition rate. At a distance $z = 79.5$ m, the pulses return to their original shape, and the process repeats itself. Note that, unlike the traditional Talbot effect where the original pulse train reforms twice in a given cycle, the pulse train in Fig. 4 reforms only once before the process repeats. This is a result of the π -phase shift, which prevents self-imaging halfway from the full cycle.

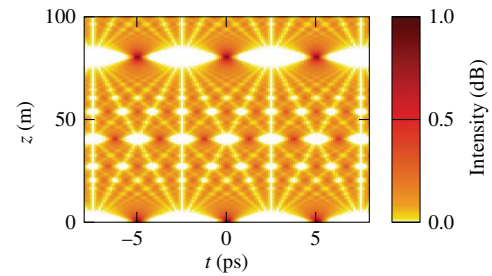


Fig. 4. Evolution of a train of sech-shaped pulses ($T_0 = 0.2$ ps) with an initial separation of 5 ps. Adjacent pulses differ in phase by π .

Figure 5 shows the evolution of the shape [Fig. 5(a)] and spectrum [Fig. 5(b)] of a single sech-shaped pulse ($T_0 = 0.2$ ps) propagating through a dispersive medium ($\beta_2 = 0.05$ ps²/m) when it is confined to a 5 ps wide temporal window formed by two refractive-index boundaries with $\beta_B = 5$ m⁻¹. In Fig. 5(a), we see that the pulse quickly broadens to fill the entire window and begins to interfere with the reflecting pulses formed at the two edges through TIR. Multiple reflections lead to a more-complicated interference pattern that begins to form progressively fewer pulses at specific distances until two pulses are formed at a distance of about 42 m. This process reverses itself, and a single pulse is reformed at $z = 85$ m (self-imaging). Figure 5(b) shows that the reflected frequencies overlap with the initial pulse spectrum, causing a spectral interference pattern that changes during propagation. Eventually, the spectrum returns to its original shape at the same distance where the pulse is self-imaged. For longer propagation lengths, the whole process repeats itself periodically, just as required by the Talbot effect.

Although the pulse evolution in Fig. 5 is very similar to that in Fig. 4, the two are not identical. In particular, the distance

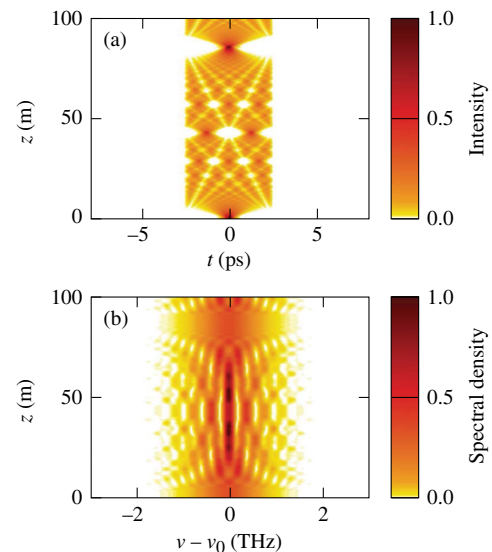


Fig. 5. Evolution of the (a) shape and (b) spectrum of a sech-shaped pulse ($T_0 = 0.3$ ps) confined to a 5 ps window through two temporal boundaries.

over which the pulse is reimaged is slightly longer in the single-pulse case. This is again related to the fact that TIR does not produce a precise phase shift of π across the entire pulse spectrum. As we saw in Eq. (18), the TIR-induced phase shift is frequency dependent. In Section 3, this frequency-dependent phase shift led to a slightly different interference pattern. If we perform the simulation in Fig. 4 again but apply the phase shift in Eq. (18), we find that the pattern matches perfectly the one shown in Fig. 5(a). Finally, we note that self-imaging in Fig. 5 is not perfect, with the reformed pulse being slightly different from the original. By increasing the value of β_B , however, the difference between the original and reformed pulses can be reduced, resulting in nearly perfect self-imaging. This makes sense because the larger the value of β_B , the closer the reflection phase shift in Eq. (18) to π over the entire bandwidth of the optical pulse.

5. CONCLUSIONS

We have shown, both numerically and analytically, that temporal reflections from a moving refractive-index boundary act as an analog of Lloyd's mirror, allowing a single pulse to produce interference fringes in time as it propagates inside a dispersive medium with a temporal boundary across which the refractive index of the medium changes. Our numerical simulations show that the pulse spectrum also develops a multipeak structure in this situation. By comparing the temporal fringe pattern to that formed through two-pulse interference, we show that temporal reflection produces a frequency-dependent phase shift that varies between 0 and π . We used the boundary conditions across the temporal boundary to derive an explicit expression for the amplitude reflection coefficient when TIR occurs and found the frequency-dependent phase shift given in Eq. (18). Applying this phase shift to a virtual second pulse produces the same interference pattern as the pulse reflecting from the temporal boundary. This matches the behavior of traditional reflection, where the reflection can be interpreted as coming from a virtual source.

We also discussed the self-imaging occurring when a second temporal boundary is added, forming a temporal waveguide that confines an optical pulse inside it. In this case, a single pulse experiences multiple reflected pulses that interfere and form a complex fringe pattern before eventually forming an image of the original pulse. This self-imaging effect is also seen in spatial planar waveguides and is similar to the temporal Talbot effect [39], which requires interference from an infinite train of pulses. Although the reimaging is not exact in general, increasing the refractive-index change across the boundary causes the reimaged pulse to more closely match the shape of the initial pulse. This arrangement could be used to selectively convert a single pulse into two or more pulses, with the number of pulses set by the length of the dispersive medium.

An experimental realization of this effect would be of great interest. One approach would involve using a pump-probe configuration, where the pump produces the moving refractive-index boundaries through cross-phase modulation. While our current discussion did not include the effects of third-order dispersion, our previous work has shown that higher-order dispersion can be largely ignored by working far from the

zero-dispersion wavelength [40]. Working near the zero-dispersion wavelength could allow for even more interesting interference patterns, as multiple reflections can occur from a single boundary.

Funding. University of Rochester (UR); Department of Energy, National Nuclear Security Administration (NNSA) (DE-NA0001944); New York State Energy Research and Development Authority (NYSERDA); National Science Foundation (NSF) (ECCS-1505636).

Acknowledgment. This paper was prepared as an account of work sponsored by an agency of the U.S. Government. Neither the U.S. Government nor any agency thereof, nor any of their employees, makes any warranty, express or implied, or assumes any legal liability or responsibility for the accuracy, completeness, or usefulness of any information, apparatus, product, or process disclosed, or represents that its use would not infringe privately owned rights. Reference herein to any specific commercial product, process, or service by trade name, trademark, manufacturer, or otherwise does not necessarily constitute or imply its endorsement, recommendation, or favoring by the U.S. Government or any agency thereof. The views and opinions of authors expressed herein do not necessarily state or reflect those of the U.S. Government or any agency thereof.

REFERENCES

1. M. Born and E. Wolf, *Principles of Optics: Electromagnetic Theory of Propagation, Interference, and Diffraction of Light*, 7th expanded ed. (Cambridge University, 1999).
2. B. Kolner, "Space-time duality and the theory of temporal imaging," *IEEE J. Quantum Electron.* **30**, 1951–1963 (1994).
3. J. Azaña, L. R. Chen, M. A. Muriel, and P. W. E. Smith, "Experimental demonstration of real-time Fourier transformation using linearly chirped fibre Bragg gratings," *Electron. Lett.* **35**, 2223–2224 (1999).
4. M. A. Muriel, J. Azaña, and A. Carballar, "Real-time Fourier transformer based on fiber gratings," *Opt. Lett.* **24**, 1–3 (1999).
5. J. T. Mendonça and P. K. Shukla, "Time refraction and time reflection: two basic concepts," *Phys. Scripta* **65**, 160–163 (2002).
6. N. N. Rozanov, "Transformation of electromagnetic radiation at moving inhomogeneities of a medium," *J. Exp. Theor. Phys. Lett.* **88**, 501–504 (2008).
7. N. N. Rozanov, "Transformation of electromagnetic radiation by rapidly moving inhomogeneities of a transparent medium," *J. Exp. Theor. Phys.* **108**, 140–148 (2009).
8. B. W. Plansinis, W. R. Donaldson, and G. P. Agrawal, "What is the temporal analog of reflection and refraction of optical beams?" *Phys. Rev. Lett.* **115**, 183901 (2015).
9. S. C. Wilks, J. M. Dawson, W. B. Mori, T. Katsouleas, and M. E. Jones, "Photon accelerator," *Phys. Rev. Lett.* **62**, 2600–2603 (1989).
10. J. T. Mendonça, *Theory of Photon Acceleration*, Plasma Physics Series (Institute of Physics, 2001).
11. T. G. Philbin, C. Kulewicz, S. J. Robertson, S. Hill, F. König, and U. Leonhardt, "Fiber-optical analog of the event horizon," *Science* **319**, 1367–1370 (2008).
12. F. Belgiorno, S. L. Cacciatori, M. Clerici, V. Gorini, G. Ortenzi, L. Rizzi, E. Rubino, V. G. Sala, and D. Faccio, "Hawking radiation from ultrashort laser pulse filaments," *Phys. Rev. Lett.* **105**, 203901 (2010).
13. E. Rubino, F. Belgiorno, S. L. Cacciatori, M. Clerici, V. Gorini, G. Ortenzi, L. Rizzi, V. G. Sala, M. Kolesik, and D. Faccio, "Experimental evidence of analogue Hawking radiation from ultrashort laser pulse filaments," *New J. Phys.* **13**, 085005 (2011).

14. D. Faccio, "Laser pulse analogues for gravity and analogue Hawking radiation," *Contemp. Phys.* **53**, 97–112 (2012).
15. D. Faccio, T. Arane, M. Lamperti, and U. Leonhardt, "Optical black hole lasers," *Class. Quantum Grav.* **29**, 224009 (2012).
16. M. Jacquet and F. König, "Quantum vacuum emission from a refractive-index front," *Phys. Rev. A* **92**, 023851 (2015).
17. M. F. Linder, R. Schützhold, and W. G. Unruh, "Derivation of Hawking radiation in dispersive dielectric media," *Phys. Rev. D* **93**, 104010 (2016).
18. A. V. Gorbach and D. V. Skryabin, "Bouncing of a dispersive pulse on an accelerating soliton and stepwise frequency conversion in optical fibers," *Opt. Express* **15**, 14560–14565 (2007).
19. A. V. Gorbach and D. V. Skryabin, "Theory of radiation trapping by the accelerating solitons in optical fibers," *Phys. Rev. A* **76**, 053803 (2007).
20. S. Hill, C. E. Kuklewicz, U. Leonhardt, and F. König, "Evolution of light trapped by a soliton in a microstructured fiber," *Opt. Express* **17**, 13588–13601 (2009).
21. S. Robertson and U. Leonhardt, "Frequency shifting at fiber-optical event horizons: the effect of Raman deceleration," *Phys. Rev. A* **81**, 063835 (2010).
22. A. Demircan, S. Amiranashvili, and G. Steinmeyer, "Controlling light by light with an optical event horizon," *Phys. Rev. Lett.* **106**, 163901 (2011).
23. A. Choudhary and F. König, "Efficient frequency shifting of dispersive waves at solitons," *Opt. Express* **20**, 5538–5546 (2012).
24. E. Rubino, A. Lotti, F. Belgiorno, S. L. Cacciatori, A. Couairon, U. Leonhardt, and D. Faccio, "Soliton-induced relativistic-scattering and amplification," *Sci. Rep.* **2**, 932 (2012).
25. L. Tartara, "Frequency shifting of femtosecond pulses by reflection at solitons," *IEEE J. Quantum Electron.* **48**, 1439–1442 (2012).
26. R. Driben, A. V. Yulin, A. Efimov, and B. A. Malomed, "Trapping of light in solitonic cavities and its role in the supercontinuum generation," *Opt. Express* **21**, 19091–19096 (2013).
27. A. V. Yulin, R. Driben, B. A. Malomed, and D. V. Skryabin, "Soliton interaction mediated by cascaded four wave mixing with dispersive waves," *Opt. Express* **21**, 14481–14486 (2013).
28. E. Hecht, *Optics*, 4th ed. (Addison-Wesley, 2002).
29. X. Li, Y. Shimizu, S. Ito, W. Gao, and L. Zeng, "Fabrication of diffraction gratings for surface encoders by using a Lloyd's mirror interferometer with a 405 nm laser diode," *Proc. SPIE* **8759**, 87594Q (2013).
30. E. B. Hochberg and N. L. Chrien, "Lloyd's mirror for MTF testing of MISR CCD," *Proc. SPIE* **2830**, 274–285 (1996).
31. J. G. Bolton, G. J. Stanley, and O. B. Slee, "Positions of three discrete sources of galactic radio-frequency radiation," in *Classics in Radio Astronomy* (Springer, 1982), pp. 239–241.
32. B. W. Plansinis, W. R. Donaldson, and G. P. Agrawal, "Temporal waveguides for optical pulses," *J. Opt. Soc. Am. B* **33**, 1112–1119 (2016).
33. G. P. Agrawal, *Nonlinear Fiber Optics*, 5th ed. (Elsevier, 2013).
34. T. Jansson, "Real-time Fourier transformation in dispersive optical fibers," *Opt. Lett.* **8**, 232–234 (1983).
35. R. W. Boyd, *Nonlinear Optics* (Academic, 2003).
36. S. Finazzi and I. Carusotto, "Quantum vacuum emission in a nonlinear optical medium illuminated by a strong laser pulse," *Phys. Rev. A* **87**, 023803 (2013).
37. S. Finazzi and R. Parentani, "Hawking radiation in dispersive theories, the two regimes," *Phys. Rev. D* **85**, 124027 (2012).
38. Z. Deng, X. Fu, J. Liu, C. Zhao, and S. Wen, "Trapping and controlling the dispersive wave within a solitonic well," *Opt. Express* **24**, 10302–10312 (2016).
39. J. Azaña and M. A. Muriel, "Technique for multiplying the repetition rates of periodic trains of pulses by means of a temporal self-imaging effect in chirped fiber gratings," *Opt. Lett.* **24**, 1672–1674 (1999).
40. B. W. Plansinis, W. R. Donaldson, and G. P. Agrawal, "Spectral splitting of optical pulses inside a dispersive medium at a temporal boundary," *IEEE J. Quantum Electron.* **52**, 6100708 (2016).